doi:10.1038/nature05601

LETTERS

Hippocampal remapping and grid realignment in entorhinal cortex

Marianne Fyhn[1]*, Torkel Hafting[1]*, Alessandro Treves[1,2], May-Britt Moser[1] & Edvard I. Moser[1]

A fundamental property of many associative memory networks is the ability to decorrelate overlapping input patterns before information is stored[1–5]. In the hippocampus, this neuronal pattern separation is expressed as the tendency of ensembles of place cells[6] to undergo extensive 'remapping' in response to changes in the sensory or motivational inputs to the hippocampus[7–13]. Remapping is expressed under some conditions as a change of firing rates in the presence of a stable place code ('rate remapping')[14], and under other conditions as a complete reorganization of the hippocampal place code in which both place and rate of firing take statistically independent values ('global remapping')[14]. Here we show that the nature of hippocampal remapping can be predicted by ensemble dynamics in place-selective grid cells in the medial entorhinal cortex[15,16], one synapse upstream of the hippocampus. Whereas rate remapping is associated with stable grid fields, global remapping is always accompanied by a coordinate shift in the firing vertices of the grid cells. Grid fields of co-localized medial entorhinal cortex cells move and rotate in concert during this realignment. In contrast to the multiple environment-specific representations coded by place cells in the hippocampus, local ensembles of grid cells thus maintain a constant spatial phase structure, allowing position to be represented and updated by the same translation mechanism in all environments encountered by the animal.

Hippocampal place representations may be derived from a metric representation of space in the medial entorhinal cortex (MEC)[15–20]. A key cell type of the MEC is the grid cell, the spatial receptive fields form a regularly tessellating triangular pattern that spans the complete environment covered by the animal[16]. The periodic firing fields of neighbouring grid cells are offset relative to each other in an apparently random manner, such that all locations within the repeating unit of the triangular lattice are represented by any sufficiently large local cell ensemble[16]. To determine how neural activity in grid cells is organized at the ensemble level and how their organization might influence the formation of representations downstream in the hippocampus, we recorded the simultaneous activity of multiple grid cells in layer II of MEC in rats (*Rattus norvegicus*) under conditions in which place cells in the hippocampus undergo global remapping or rate remapping[14] (Fig. 1, Supplementary Figs 1 and 2, Supplementary Methods and Supplementary Tables 1–3). Cells were recorded simultaneously from MEC and area CA3 in 5 out of 15 rats with MEC electrodes. Global remapping was induced by two different procedures, one in which the rat was tested in the same location in either a square or a circular enclosure[7,9,21,22] (Fig. 1a) and another in which the animal alternated between similar square boxes in two different rooms[6,13,14] (Fig. 1b). These protocols induced pronounced changes in firing rate and firing location throughout the place cell population in all experiments in which CA3 cells were recorded (7 rats; 15 experiments; Fig. 1d–g). Rate remapping was induced by changing the walls of a square recording enclosure from a three black and one white configuration to a one black and three white configuration[14] (Fig. 1c). This induced consistent rate remapping in all seven experiments in which CA3 cells were recorded (five rats; Fig. 1d, e, h).

With distinct protocols for inducing global remapping and rate remapping in the hippocampus, we examined the collective neuronal firing patterns of grid cells in MEC in 21 experiments with 5 or more grid cells recorded simultaneously from the dorsocaudal part of MEC. Population dynamics in entorhinal grid cells was found to be strongly predictive of the type of remapping induced in the hippocampus. When global remapping was evoked by replacing the square box with the circular box, the cross-correlograms for individual grid cells (Fig. 2b, top) as well as simultaneously recorded ensembles (Fig. 2b, bottom) formed triangular grid-like patterns, suggesting that grid spacing, grid orientation and spatial phase distribution were preserved between the conditions (Fig. 2c, d). However, in all seven experiments using this protocol, the peak of the entorhinal cross-correlogram was offset from the origin when trials in different environments were compared. The offset was similar in all simultaneously recorded grid cells (Supplementary Figs 3–5). Between experiments, the displacement ranged from 10.0 to 23.8 cm, with the upper parts of the range corresponding to nearly one-half of the grid spacing at the recording location (red vectors in Fig. 2e; Supplementary Table 2 and Supplementary Figs 3c and 6). The displacement was significantly larger than between repeated trials in the same box (range 0.1–2.3 cm; blue vectors in Fig. 2e; $Z = 2.4$, $P < 0.01$, one-tailed Wilcoxon signed-ranks test). The direction of the offset was uniformly distributed between experiments (Fig. 2e; $r = 0.34$, $P > 0.05$, Rayleigh test for randomness). When cells were recorded from the same location over several days, the distance and the direction of the grid shift remained constant (Supplementary Fig. 3d). In three out of seven animals, the grid also showed a weak expansion from the square to the circle. The expansion was coherent among simultaneously recorded cells (Supplementary Fig. 5a and Supplementary Table 2). Cross-correlograms for simultaneously recorded CA3 cells were essentially flat (Fig. 2f and Supplementary Fig. 6), as would be expected if both firing location and firing rate are orthogonalized in CA3. These observations indicate that during global remapping in the hippocampus, the map of grid cells in the MEC realigns with changes in the environment without losing its intrinsic spatial phase structure.

To determine whether ensembles of grid cells remain coherent with more substantial changes in the external input, we compared the spatial phase relationship of simultaneously recorded grid cells during foraging in rooms with different distal landmarks (rooms A and B). Although the grid structure of individual cells was maintained across rooms, the periodicity was not immediately visible in

[1]Centre for the Biology of Memory, Norwegian University of Science and Technology, NO-7489 Trondheim, Norway. [2]Cognitive Neuroscience Sector, SISSA International School for Advanced Studies, I-34014 Trieste, Italy.
*These authors contributed equally to this work.

the population cross-correlograms (Fig. 3a–c). However, peaks became apparent when one stack was rotated, in steps of 3°, relative to the other (Fig. 3c, d, and Supplementary Figs 3e–g, 4 and 7). Maximal correlation was obtained for rotations ranging from 66° clockwise to 78° counterclockwise. With optimal rotation, the displacement of the population grid ranged from 5.7 to 27.5 cm (Fig. 3e, red vectors). The direction of the offset was uniformly distributed ($r = 0.60$, $P > 0.05$, Rayleigh test for randomness). On repeated trials in the same room (A versus A′), the peak of the cross-correlogram remained in the centre (range of displacements 0–2.3 cm; Fig. 3e, blue vectors). The shift between room A and room B, with optimal rotation, was significantly larger than that between repeated trials in the same room ($Z = 2.5$, $P < 0.01$). In five out of eight ensembles, the grid spacing was slightly different between rooms A and B (Supplementary Table 2); in those cases, the scaling was coherent between simultaneously recorded neurons (Supplementary Fig. 5c). Cross-correlograms for ensembles of CA3 cells in rooms A and B were flat (Fig. 3f and Supplementary Fig. 7). These observations suggest that grid fields moved and rotated, and sometimes expanded or contracted, when the rat was moved to a new location, but the intrinsic spatial phase structure of the grid cells was maintained. This differs from the orthogonalized representations of CA3 and indicates a possible pattern separation mechanism in the entorhinal inputs to the hippocampus.

We verified these results by examining whether ensemble activity in MEC was coherent in the temporal domain. Using only rats with simultaneous recordings from MEC and CA3, we compared the distribution of temporal population vectors, with population vectors defined as lists of cells that fired together across bins of 150 ms throughout the trial[13]. In MEC, the mean Shannon mutual information between trial and population vectors was no larger for comparisons of trials in different geometric shapes than for comparisons of

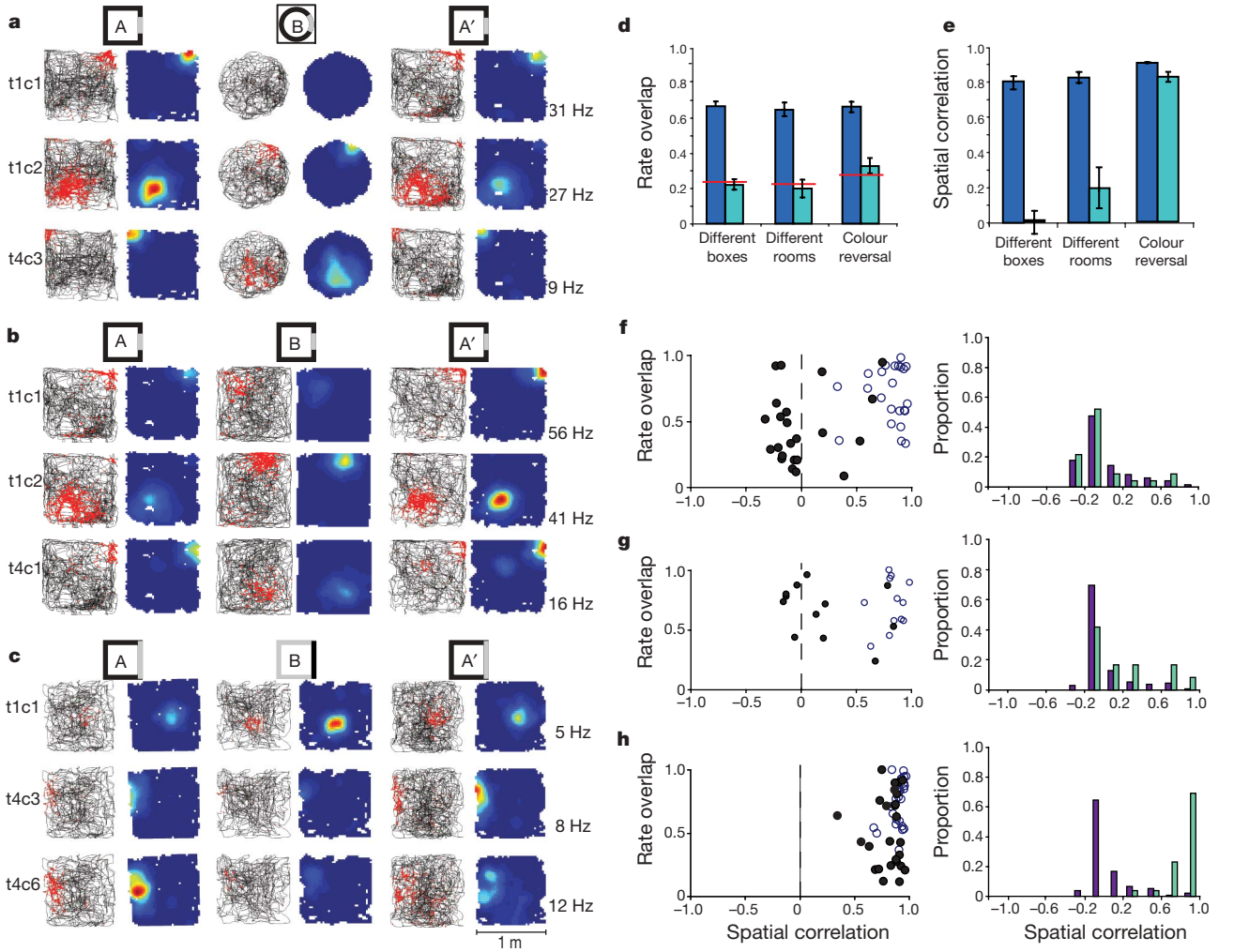

Figure 1 | Procedures for inducing global remapping and rate remapping in hippocampal area CA3. **a**–**c**, Firing fields of three simultaneously recorded CA3 cells during global remapping (different boxes in a constant location (**a**) or similar boxes in different rooms (**b**)) or rate remapping (different wall colours (**c**)). For complete cell samples see Supplementary Fig. 2a–f. Each row shows data from one active neuron (t, tetrode; c, cell). Each pair of columns shows, for each neuron, the location of spikes (red) on the trajectory of the rat (left) and a colour-coded map of the firing rate distribution (right; dark blue is zero, red is maximum; peak rate is indicated). **d**, Change in firing rates estimated by rate overlap (means ± s.e.m.). Red lines indicate chance levels. Blue bars, same environment (A–A′); green bars, different environments (A–B). **e**, Spatial correlation for cells with activity in both environments (means ± s.e.m.; best rotation). **f**–**h**, Rate overlap and spatial correlation in cells with activity in both environments. **f**, Different boxes (as in **a**); **g**, different rooms (as in **b**); **h**, different colours (as in **c**). Scatter plots show rate overlap as a function of spatial correlation for individual CA3 cells (open circles, A versus A′; filled circles, A versus B). Frequency distributions show spatial correlations (green bars) compared with distributions for shuffled cell pairs (purple bars) from the same experiments. In the different-boxes task, 2 out of 23 spatial correlations exceeded the upper limit of the 95% confidence interval of the shuffled distribution. In the different-rooms task, 3 out of 12 correlations were outside the 95% confidence interval. In the rate remapping task, 25 out of 26 cells were outside the 95% confidence interval. The rate overlap between A and B is significantly higher in **f**–**h** than in **d** because the scatter plots in **f**–**h** do not include the large number of cells with low rates in one of the environments.

repeated trials in the same shape, and no larger for different rooms than for repeated trials in the same room (Supplementary Fig. 8; $t < 1.1$, $P > 0.05$, one-tailed paired t-tests), indicating that grid cells that are coactive in one environment may remain coactive in other environments too. In CA3, information about trial type was above 0.5 bits for square versus circle trials as well as trials in different rooms, significantly above the values obtained for repeated tests in the same environment (Supplementary Fig. 8; square versus circle: $t(7) = 5.6$, $P < 0.001$; two rooms: $t(4) = 3.8$, $P < 0.01$). The differentiation of coactivity patterns in CA3 further reinforces the view that incoming sensory input is decorrelated as it enters the hippocampus during global remapping.

In striking contrast with the coordinate shift during global remapping, grid vertices remained stable when place cells exhibited rate remapping, such as when the box colours were reversed. The peak of the cross-correlogram for trials with different colour configurations remained in the centre for six out of seven experiments (displacement 0–2.7 cm) and was slightly offset (7.1 cm) in one experiment (Fig. 4b, c, and Supplementary Figs 3h, i and 9). The peak displacement after colour reversal was not significantly different from the displacement observed in the same cells on trial pairs with identical colours (range 0–1.3 cm; $Z = 1.4$, $P > 0.05$). There was no change in the scale of the grid between 'black' and 'white' trials (Supplementary Table 2). There was also no significant change in the location of the cross-correlation peak in CA3 (median shift of 6.3 cm after colour reversal, in contrast with 4.9 cm with similar colours; $Z = 0.7$, not significant; Fig. 4d). Rate remapping in the hippocampus was not associated with significant rate changes between the individual grid fields of the entorhinal neurons (Supplementary Fig. 10).

We finally examined whether global remapping in the hippocampus and grid realignment in the entorhinal cortex are coincident, because strong temporal contiguity would be expected if the phenomena were mechanistically related. Three rats, two of which had electrodes in both MEC and CA3, were trained in a square enclosure with lights on and off on alternating discrete sessions. The procedure induced global remapping between dark and light trials during the training phase in both rats with hippocampal electrodes (Supplementary Fig. 11a, b)[23]. The simultaneously recorded entorhinal representation was coherent but displaced and rotated between the trials. To evoke instantaneous global remapping, the room lights were turned on after 11 min of running in the dark condition on the test day. In one animal this caused a sudden reversion to the original hippocampal map associated with the light condition. This instance of global hippocampal remapping coincided with an equally fast realignment of the entorhinal map, expressed as a loss of spatial correlation between grid fields recorded before and after the light was turned on (Supplementary Fig. 11a, c). In the second rat, all hippocampal and entorhinal neurons maintained their firing fields when the darkness was terminated[23], presumably reflecting a continued influence of self-motion information on the location of firing in grid cells and place cells[16]. To reset the path integrator, the rat was lifted up on a pedestal for 1 min. The temporary disruption of running caused an immediate reversion to the original hippocampal map, associated with the light condition, when the rat was returned to the box. At the same time, a coherent shift and rotation of the population grid was

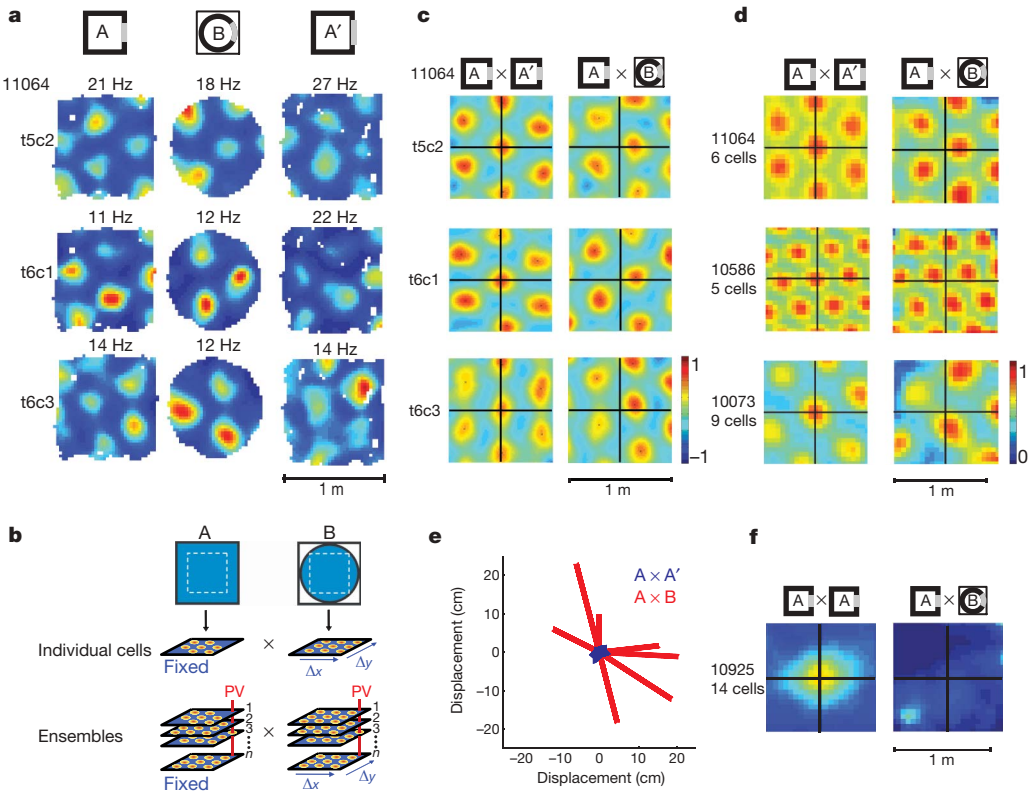

Figure 2 | Realignment of entorhinal grid fields during hippocampal global remapping between different boxes in the same location. **a**, Colour-coded firing rate maps for three representative simultaneously recorded MEC cells (a complete cell sample is given in Supplementary Fig. 3a). Five-digit numbers (for example 11064) refer to rat identities. **b**, Schematic illustration of the procedure for cross-correlation of rate maps based on individual rate maps (top) or stacks of rate maps (bottom). Cross-correlation matrices were determined by shifting the two maps relative to one another in steps of 5 cm in both the x and y directions within the common stippled area. PV, population vector (defined for each 5×5 cm^2 bin). **c**, **d**, Colour-coded cross-correlation matrices for representative individual cells (**c**; same cells as in **a**) and cell ensembles (**d**) during repeated testing in the same box (A versus A′) or in different boxes (A versus B) (for all other experiments see Supplementary Fig. 3c). **e**, Vector diagram showing distribution across experiments of the direction and the distance of the grid displacement, measured from the origin to the nearest peak of the cross-correlogram. **f**, Representative cross-correlogram for CA3 ensembles.

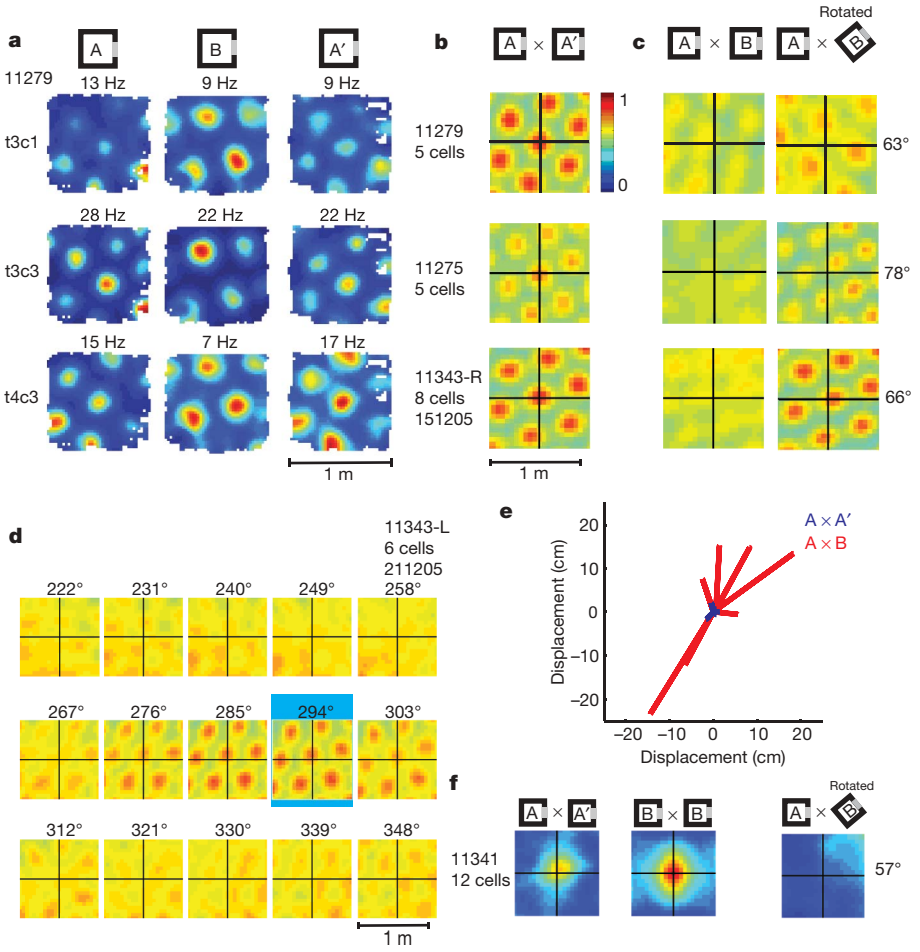

Figure 3 | Realignment of entorhinal grid fields during hippocampal global remapping between two rooms. **a**, Rate maps for representative simultaneously recorded MEC cells (a complete cell sample is given in Supplementary Fig. 3e). **b**, **c**, Cross-correlation matrices for representative grid cell ensembles. **b**, Repeated trials in room A (A–A′); **c**, room A versus room B. The right column in **c** shows cross-correlograms for the rotation that gave maximal grid structure (left column, no rotation). For all other experiments see Supplementary Fig. 3f, g. **d**, Cross-correlogram for incremental amounts of rotation in one experiment (blue, maximal correlation). **e**, Vector diagram showing distribution across experiments of direction and distance of grid displacement after optimal rotation. **f**, Representative cross-correlograms for simultaneously recorded CA3 pyramidal cells.

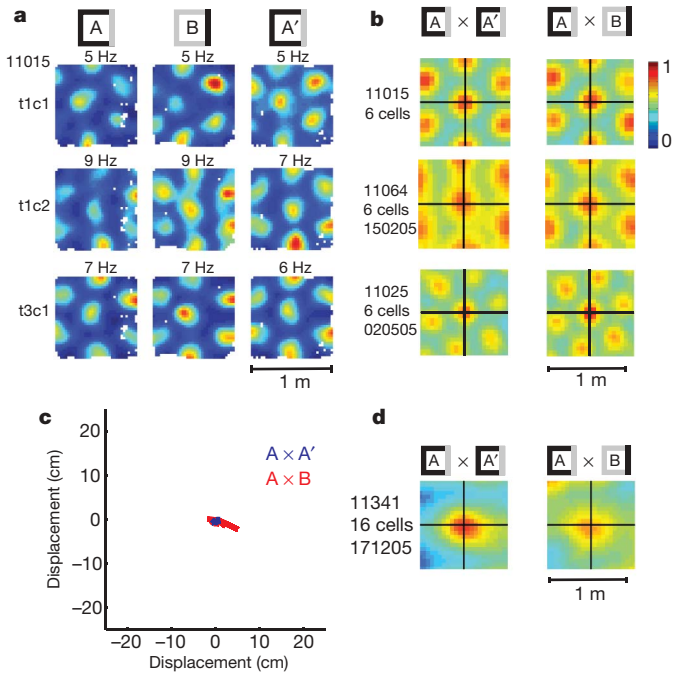

observed in MEC. The coincidence of the changes in entorhinal and hippocampal population dynamics in the two animals indicates that the changes may be part of a single integrated process.

First, these results indicate that local ensembles of grid cells may have a rigid spatial phase relationship. The repetition of the same sequence of active units as an animal follows a similar route in different arenas supports the hypothesis that the grid network is a universal metric for path-integration-based navigation[16,19,24–26]. Second, the association between hippocampal global remapping and entorhinal grid realignment implies network dynamics in the MEC as a possible determinant of orthogonalization processes in hippocampal place cells (Supplementary Fig. 12). The stability of entorhinal grid cells during rate remapping in the hippocampus raises the possibility that the rate orthogonalization originates in the dentate gyrus and CA3 (ref. 27), perhaps as a consequence of convergence between

Figure 4 | Unaltered alignment of entorhinal grid fields during rate remapping in CA3. **a**, Rate maps for representative simultaneously recorded grid cells in the different-colours task (a complete cell sample is given in Supplementary Fig. 3h). **b**, Cross-correlation maps for representative grid cell ensembles (for all other experiments see Supplementary Fig. 3i). Left column, trials with similar wall colours (A–A′); right, trials with different wall colours (A–B). **c**, Vector diagram showing distribution across experiments of direction and distance of grid displacement. **d**, Representative cross-correlogram for CA3 ensembles.

spatial signals from grid cells in MEC and nonspatial signals from neurons in the lateral entorhinal cortex[28,29]. The possible recoding of spatial information from a single, universal neural representation in the entorhinal cortex onto statistically independent context-sensitive cell ensembles in high-capacity networks of the hippocampus[30] is probably crucial for the successful storage of episodic memory (see Supplementary Discussion).

METHODS

Neuronal ensemble activity was recorded with tetrodes in 19 Long Evans rats implanted with microdrives in dorsocaudal MEC and/or dorsal CA3 of the hippocampus. Spike-triggered activity was sampled in blocks of 10 or 20 min while rats chased soft food crumbs in familiar enclosures of different shapes, textures and colours. Global remapping was induced by alternating between square and circular recording enclosures at a constant location within the same room, by testing the rat in similar square boxes in two rooms with distinct background cues[13], or by training the rat on separate trials in the same environment in light and darkness[23]. Rate remapping was induced by training the animals in a square enclosure with exchangeable walls of different colour[14]. Detailed experimental and analytical procedures are provided in Supplementary Methods.

Received 4 July 2006; accepted 15 January 2007.
Published online 25 February 2007.

1. Marr, D. Simple memory: a theory of archicortex. *Phil. Trans. R. Soc. Lond. B* **262,** 23–81 (1971).
2. McNaughton, B. L. & Nadel, L. in *Neuroscience and Connectionist Theory* (eds Gluck, M. A. & Rumelhart, D. E.) 1–63 (Erlbaum, Hillsdale, NJ, 1989).
3. Treves, A. & Rolls, E. T. Computational constraints suggest the need for two distinct input systems to the hippocampal CA3 network. *Hippocampus* **2,** 189–199 (1992).
4. Kesner, R. P., Gilbert, P. E. & Wallenstein, G. V. Testing neural network models of memory with behavioral experiments. *Curr. Opin. Neurobiol.* **10,** 260–265 (2000).
5. Leutgeb, S., Leutgeb, J. K., Moser, M.-B. & Moser, E. I. Place cells, spatial maps and the population code for memory. *Curr. Opin. Neurobiol.* **15,** 738–746 (2005).
6. O'Keefe, J. & Nadel, L. *The Hippocampus as a Cognitive Map* (Clarendon, Oxford, 1978).
7. Bostock, E., Muller, R. U. & Kubie, J. L. Experience-dependent modifications of hippocampal place cell firing. *Hippocampus* **1,** 193–205 (1991).
8. Markus, E. J. *et al.* Interactions between location and task affect the spatial and directional firing of hippocampal neurons. *J. Neurosci.* **15,** 7079–7094 (1995).
9. Kentros, C. *et al.* Abolition of long-term stability of new hippocampal place cell maps by NMDA receptor blockade. *Science* **280,** 2121–2126 (1998).
10. Wood, E. R., Dudchenko, P. A., Robitsek, R. J. & Eichenbaum, H. Hippocampal neurons encode information about different types of memory episodes occurring in the same location. *Neuron* **27,** 623–633 (2000).
11. Frank, L. M., Brown, E. N. & Wilson, M. Trajectory encoding in the hippocampus and entorhinal cortex. *Neuron* **27,** 169–178 (2000).
12. Lever, C., Wills, T., Cacucci, F., Burgess, N. & O'Keefe, J. Long-term plasticity in hippocampal place-cell representation of environmental geometry. *Nature* **416,** 90–94 (2002).
13. Leutgeb, S., Leutgeb, J. K., Treves, A., Moser, M.-B. & Moser, E. I. Distinct ensemble codes in hippocampal areas CA3 and CA1. *Science* **305,** 1295–1298 (2004).
14. Leutgeb, S. *et al.* Independent codes for spatial and episodic memory in the hippocampus. *Science* **309,** 619–623 (2005).
15. Fyhn, M., Molden, S., Witter, M. P., Moser, E. I. & Moser, M.-B. Spatial representation in the entorhinal cortex. *Science* **305,** 1258–1264 (2004).
16. Hafting, T., Fyhn, M., Molden, S., Moser, M.-B. & Moser, E. I. Microstructure of a spatial map in the entorhinal cortex. *Nature* **436,** 801–806 (2005).
17. Steffenach, H.-A., Witter, M. P., Moser, M.-B. & Moser, E. I. Spatial memory in the rat requires the dorsolateral band of the entorhinal cortex. *Neuron* **45,** 301–313 (2005).
18. Sargolini, F. *et al.* Conjunctive representation of position, direction and velocity in entorhinal cortex. *Science* **312,** 754–758 (2006).
19. McNaughton, B. L., Battaglia, F. P., Jensen, O., Moser, E. I. & Moser, M.-B. Path integration and the neural basis of the 'cognitive map'. *Nature Rev. Neurosci.* **7,** 663–678 (2006).
20. Solstad, T., Moser, E. I. & Einevoll, G. T. From grid cells to place cells: a mathematical model. *Hippocampus* **16,** 1026–1031 (2006).
21. Wills, T. J., Lever, C., Cacucci, F., Burgess, N. & O'Keefe, J. Attractor dynamics in the hippocampal representation of the local environment. *Science* **308,** 873–876 (2005).
22. Anderson, M. I. & Jeffery, K. J. Heterogeneous modulation of place cell firing by changes in context. *J. Neurosci.* **23,** 8827–8835 (2003).
23. Quirk, G. J., Muller, R. U. & Kubie, J. L. The firing of hippocampal place cells in the dark depends on the rat's recent experience. *J. Neurosci.* **10,** 2008–2017 (1990).
24. Redish, A. D. & Touretzky, D. S. Cognitive maps beyond the hippocampus. *Hippocampus* **7,** 15–35 (1997).
25. Sharp, P. E. Complimentary roles for hippocampal versus subicular/entorhinal place cells in coding place, context, and events. *Hippocampus* **9,** 432–443 (1999).
26. Fuhs, M. C. & Touretzky, D. S. A spin glass model of path integration in rat medial entorhinal cortex. *J. Neurosci.* **26,** 4266–4276 (2006).
27. Leutgeb, J. K., Leutgeb, S., Moser, M.-B. & Moser, E. I. Pattern separation in dentate gyrus and CA3 of the hippocampus. *Science* **315,** doi:10.1126/science.1135801 (16 February 2007)
28. Hargreaves, E. L., Rao, G., Lee, I. & Knierim, J. J. Major dissociation between medial and lateral entorhinal input to the dorsal hippocampus. *Science* **308,** 1792–1794 (2005).
29. Naber, P. A., Caballero-Bleda, M., Jorritsma-Byham, B. & Witter, M. P. Parallel input to the hippocampal memory system through peri- and postrhinal cortices. *Neuroreport* **8,** 2617–2621 (1997).
30. Battaglia, F. P. & Treves, A. Attractor neural networks storing multiple space representations: a model for hippocampal place fields. *Phys. Rev. E Stat. Phys. Plasmas Fluids Relat. Interdiscip. Top.* **58,** 7738–7753 (1998).

Supplementary Information is linked to the online version of the paper at www.nature.com/nature.

Acknowledgements We thank S. Leutgeb, T. Solstad, B. L. McNaughton and M. P. Witter for discussion, R. Skjerpeng for programming, and I. Hammer, K. Haugen, K. Jenssen and H. Waade for technical assistance. This work was supported by a Centre of Excellence grant from the Norwegian Research Council.

Author Contributions M.F., T.H., M.-B.M. and E.I.M. planned experiments and analyses. M.F., T.H. and M.-B.M. performed the experiments and analysed the data. A.T. gave advice on analyses, and E.I.M. wrote the paper. All authors discussed the results and contributed to the manuscript.

Author Information Reprints and permissions information is available at www.nature.com/reprints. The authors declare no competing financial interests. Correspondence and requests for materials should be addressed to E.I.M. (edvard.moser@ntnu.no).